Chemical Papers
https://doi.org/10.1007/s11696-024-03737-3

ORIGINAL PAPER

Antimicrobial and anti-biofilm activities of photosynthesized Ag@TiO_2 and Ag@N-TiO_2 nanocomposites against clinically isolated multidrug resistance *Klebsiella pneumoniae*

Alif Firman Firdausy[1,2] · Liszulfah Roza[3] · Mohammad Mansoob Khan[4] · Abdul Wafi[5]

Received: 27 February 2024 / Accepted: 13 October 2024

Abstract

The rise of drug-resistant bacterial strains is escalating due to the ability to produce biofilms shielding bacteria from antimicrobial agents. Consequently, novel approaches are imperative for managing biofilm-related infections in healthcare settings. Silver-based nanoparticles have revealed potential antimicrobial characteristics against various bacteria. In the present work, silver-modified TiO_2 (Ag@TiO_2) and silver-modified/N-doped TiO_2 (Ag@N-TiO_2) nanocomposites were synthesized using the sol–gel and photochemical deposition under UV light illumination. FTIR, XRD, and DRS were performed to characterize the vibrational, structural, and optical properties of the synthesized materials, respectively. In addition, FE-SEM and EDX analysis were also utilized to determine the surface morphology, particle size, and elemental composition of the prepared materials. Furthermore, the synthesized Ag@TiO_2 and Ag@N-TiO_2 nanocomposites were explored and compared for antimicrobial and anti-biofilm agents against clinically isolated multidrug-resistant (MDR) *Klebsiella pneumoniae* (*K. pneumoniae*) on the silicone rubber as a urinary catheter material in the medical devices. The results showed that both Ag@TiO_2 and Ag@N-TiO_2 composites exhibited antimicrobial activities compared to negative control. The Ag^{-3}@TiO_2 composite possessed a highest inhibition zone (77.29%) against MDR *K. pneumoniae.* In addition, anti-biofilm assay through the crystal violet method showed that Ag^{-1}@TiO_2 revealed an optimum inhibition (54.20%) compared to other samples. In conclusion, Ag@TiO_2 and Ag@N-TiO_2 nanocomposites have exhibited promising antimicrobial and anti-biofilm agents in medical devices, providing an effective inhibition toward the bacterial growth and biofilm formation of MDR *K. pneumoniae.*

Keywords Antimicrobial · Anti-biofilm · Multidrug-resistant · *Klebsiella pneumonia* · Silver-doped TiO_2 · Silver/nitrogen co-doped TiO_2

✉ Abdul Wafi
abdul.wafi.1@brin.go.id; abdulwafi.id@gmail.com

Alif Firman Firdausy
aliffirman.firdausy@uin-malang.ac.id
https://scholar.google.co.id/citations?user=f93gQLgAAAAJ&hl=en

Liszulfah Roza
lisz001@brin.go.id
https://scholar.google.co.kr/citations?user=ynzk598AAAAJ&hl=en

Mohammad Mansoob Khan
mansoob.khan@ubd.edu.bn

[1] Department of Pharmacy, Faculty of Medicine and Health Science, Universitas Islam Negeri Maulana Malik Ibrahim, Malang, Indonesia

[2] Interdisciplinary Nanoscience Center (INANO), Faculty of Natural Science, Aarhus University, Aarhus, Denmark

[3] Research Center for Nanotechnology Systems, National Research and Innovation Agency (BRIN), South Tangerang, Indonesia

[4] Chemical Sciences, Faculty of Science, Universiti Brunei Darussalam, Jalan Tungku Link, Gadong BE1410, Brunei Darussalam

[5] Research Center for Advanced Materials, National Research and Innovation Agency (BRIN), South Tangerang, Indonesia

Published online: 23 October 2024

Introduction

Klebsiella pneumoniae, a gram-negative bacterium belonging to the family of *Enterobacteriaceae,* is naturally found as normal microbiota in the human gastrointestinal tract. Uncontrollable growth of these bacteria can lead to serious multiple-site infection problems including meningitis, endophthalmitis, pyogenic liver abscess, and urinary tract infection (Chang et al. 2021; Li et al. 2022). *K. pneumoniae* can be transmitted through urinary catheters to cause healthcare-associated urinary tract infections (HAUTIs) and catheter-associated urinary tract infections (CAUTIs) (Chang et al. 2021; CDC 2024).

The spreading of antimicrobial resistance cases associated with *K. pneumoniae* infections has gotten worse in the last two decades. In 2017, the WHO categorized multidrug resistance (MDR) *Enterobacteriaceae,* including *K. pneumoniae,* on top of the list of bacteria that urgently needed new antibiotics (Tacconelli et al. 2018). These bacteria can generate multiple defensive mechanisms to avoid antimicrobial agents; one of them is biofilm production (Adeosun et al. 2022). Biofilm is a dense structure consisting of hetero-microbes living and surrounded by an exopolysaccharide matrix (Donlan 2002). This structure protects *K. pneumoniae* from unfavorable living conditions and makes them remain viable for 2 to 4 weeks on abiotic surfaces like the inner side of the catheter tube (Centeleghe et al. 2023).

Silver nanoparticles (Ag NPs) are known as inert-biologically active against broad-spectrum pathogens. It has previously been reported that Ag NPs exhibited antimicrobial mechanisms through membrane disruption by reactive oxygen species/ROS generated from photocatalytic reactions (Wafi et al. 2020; Alotaibi et al. 2022). Ag NPs combined with titanium dioxide (TiO_2) as a carrier were widely used as antimicrobial coating agents because of their stability, availability, and cost-effectiveness (Jalali et al. 2016). The addition of nitrogen (N) atom on Ag@TiO_2 nanoparticle results in shifting of excitation wavelength from a higher energy ultraviolet into a lower visible light region, hence enhancing its antimicrobial activity in living environments (Wong et al. 2015; Calisir et al. 2020). Some study of Ag@N-TiO_2 nanoparticles shows antimicrobial and anti-biofilm efficacy against some pathogens such as *Staphylococcus aureus, Escherichia coli, Vibrio fischeri,* and *Chromobacterium violaceum* (Khan et al. 2012; Naik and Kowshik 2014; Santhosh and Natarajan 2015; Wafi et al. 2020).

However, to the best of our knowledge, there is no evidence of Ag@TiO_2 and Ag@N-TiO_2 nanocomposites as novel antimicrobial and anti-biofilm agents for clinically isolated MDR *K. pneumoniae* bacteria. Hence, the anti-biofilm effect of Ag@TiO_2 and Ag@N-TiO_2 nanocomposites was also evaluated against MDR *K. pneumoniae* on a surface of silicone material. In addition, the vibrational, structural, optical, surface morphology, particle size, and elemental composition of the synthesized Ag@TiO_2 and Ag@N-TiO_2 nanocomposites were also characterized and discussed in detail.

Materials and methods

Materials

The materials used in this work were all in analytical grade. Titanium (IV) isopropoxide, TTIP ($Ti[OCH(CH_3)_2]_4$) 98%, and crystal violet 0.1% were obtained from Sigma-Aldrich. Ethanol 70%, urea, and $AgNO_3$ were obtained from Merck. Meropenem was purchased from Hexpharm. Antibiotics contained paper discs including amoxicillin (AML), cefixime (CFM), cefotaxime (CTX), cefuroxime (CXM), and ceftriaxone (CXO) were obtained from Oxoid. In addition, a Milli-Q system was used to obtain the distilled water.

Klebsiella pneumoniae strain bacteria were obtained from the sputum of a pneumonia-active patient at Dr. Saiful Anwar Hospital, Malang, Indonesia. The cultivation was taken at the Laboratory of Microbiology, Faculty of Medicine, Universitas Brawijaya, Indonesia. Microbiological grade culture media used in this study (Luria–Bertani and Mueller Hinton Agar) was purchased from HiMedia.

Synthesis of TiO_2 and N-TiO_2

The N-TiO_2 and bare TiO_2 were synthesized using the facile sol–gel method at low temperatures. Generally, 5 mL of titanium (IV) isopropoxide was dispersed in the 40 mL of ethanol under continuous stirring for 5 min. Then, 4 g of urea (as N dopant) in 10 mL distilled water was added into the mixture solution and stirred for 60 min at ambient temperature. Afterward, the suspension was heated to evaporate the ethanol then dried in the oven for 15 h at 80 °C. The white precipitate then was calcined for 30 min at 450 °C (heating rate of 5 °C min^{-1}). The bare TiO_2 was also synthesized in a similar way without urea addition.

Synthesis of Ag@TiO_2 and Ag@N-TiO_2 nanocomposites

The photochemical reduction technique was utilized to decorate the surface of TiO_2 and N-TiO_2 with Ag nanoparticles. Typically, 150 mg of the prepared bare TiO_2 or N-TiO_2 photocatalysts were dispersed in 20 mL $AgNO_3$ solution with various concentrations (10^{-1} M, 10^{-2} M, and 10^{-3} M) and homogeneously stirred for 10 min to reach equilibrium.

Subsequently, the mixtures were irradiated by using a UV lamp of 15 Watt (365 nm) to initiate the photochemical reduction of Ag^{+} into Ag^{0}. After 10 min of the photoreduction process, the mixture was filtered and obtained products were dried in the oven overnight. A gray powder of Ag@TiO_2 and Ag@N-TiO_2 was obtained and coded as Ag^{-1}@TiO_2, Ag^{-2}@TiO_2, Ag^{-3}@TiO_2, Ag^{-1}@N-TiO_2, Ag^{-2}@N-TiO_2, Ag^{-3}@N-TiO_2. Ag^{-1}, Ag^{-2}, and Ag^{-3} codes are representing the initial $AgNO_3$ concentrations of 10^{-1} M, 10^{-2} M, and 10^{-3} M, respectively. Furthermore, the collected materials were subjected to characterization, antimicrobial and anti-biofilm tests.

Characterizations

The crystalline phase and crystallite size of the prepared photocatalysts were measured using a Rigaku SmartLab X-ray diffractometer with a Cu Kα radiation source ($\lambda = 1.5405$ Å) in 2θ range from 10 to 90. Field emission scanning electron microscope (FE-SEM) Hitachi SU3500 equipped with an energy-dispersive X-ray (EDS) spectrometer was utilized to determine the surface morphology, particle size, and elemental composition of the samples. The optical properties of the photocatalysts were determined by using an Ocean Optics Inc. diffuse reflectance spectrometer (DRS). The Thermo Scientific Nicolet FTIR-ATR was used to evaluate the vibrational characteristics of the samples.

Bacterial identification and antibiotic susceptibility test

Morphological, physiological, and biochemical identification were conducted to *K. pneumoniae* isolate. The isolates were spread-streaked onto MacConkey agar plates and incubated for 24 h at 37 °C. The presence of *K. pneumoniae* was identified by its distinctive pink mucoid colonies (Osman et al. 2020). Gram staining method using crystal violet, iodine, and safranin were used to observe and identify the isolate under microscope. *K. pneumoniae* appear as a rod-shaped gram-negative bacterium. For more identification, Microbact® GNB 12A (Oxoid) biochemical test was done. Pour 4 drops of bacterial suspension into the test strip's well then placed for incubation at 35 °C for 24 h. After the incubation, briefly added 1 drop of TDA reagent (Oxoid) and recorded the results using Microbact® identification package.

Antimicrobial test

The antimicrobial activity of Ag@TiO_2 and Ag@N-TiO_2 nanocomposites was evaluated using the disc diffusion (Kirby-Bauer) method. A 200 µL of *K. pneumoniae* suspension was inoculated on MHA media. A 3 mg of Ag@TiO_2 or Ag@N-TiO_2 was transferred into 10 mL of acetone to make a 0.3 mg/L(w/v) suspension. A blank paper disc was submerged into suspension for 15 min and placed on the surface of pre-inoculated MHA media. The dish was then incubated for 24 h at 37 °C and observed. Clear circular zone around the disc is defined as inhibition zone. It was measured triplicates from edge-to-edge of inhibition zone (vertical, horizontal, and diagonally). For the comparison, 10 µg of meropenem was used for positive control and Lysogeny broth medium for negative control.

Anti-biofilm assay

Microtiter plate method was performed to measure the anti-biofilm activity of Ag@TiO_2 and Ag@N-TiO_2 nanocomposites on silicone material. Medical-grade silicone sheets with 1 mm thickness obtained from ASONE® were cut into disks with a diameter of 6 mm. Ag@TiO_2 and Ag@N-TiO_2 nanocomposites were coated on the surface of silicones. Coated silicones were placed in a 48-well microtiter plate and submerged with 200 µL of *K. pneumoniae* suspension. After 6 h of incubation at 37 °C, the biofilm formed on the surface of the well and silicone discs was stained with a 0.1% crystal violet dye solution. Firstly, the unattached bacteria in the suspension were discharged then added by 125 µL of 0.1% crystal violet solution into the well, then incubated for 15 min. Then, the solution was pulled out and rinsed using distilled water three times to remove the excess of crystal violet. Furthermore, 200 µL of 30% acetic acid was added, and the diluted crystal violet was quantified to measure the amount of biofilm. The quantification was performed using a MERCK Biotek microplate reader at 595 nm. Optical density at 595 nm (OD_{595}) was used to quantify the stained biomass on biofilm formation of *K. pneumoniae*. The higher intensity of OD_{595} shows a higher biofilm formation which means a lower inhibition (Roy et al. 2018).

Furthermore, a 10 µg of meropenem and Lysogeny broth medium were used as a positive and negative control, respectively.

Results and discussion

Material properties

Figure 1a shows the FTIR spectra of the prepared samples. Firstly, the broadband around 400–900 cm^{-1} can be assigned to the Ti-O and O-Ti-O stretching. Because of the adsorbed water, the OH stretching and bending are observed around 1627 cm^{-1} and 3000–3500 cm^{-1}, respectively (Ocwelwang and Tichagwa 2014; Cheng et al. 2016). Furthermore, the peak around 1402 cm^{-1} is assigned to the bending of N–H which is found in the N-TiO_2 and Ag@N-TiO_2 samples. In

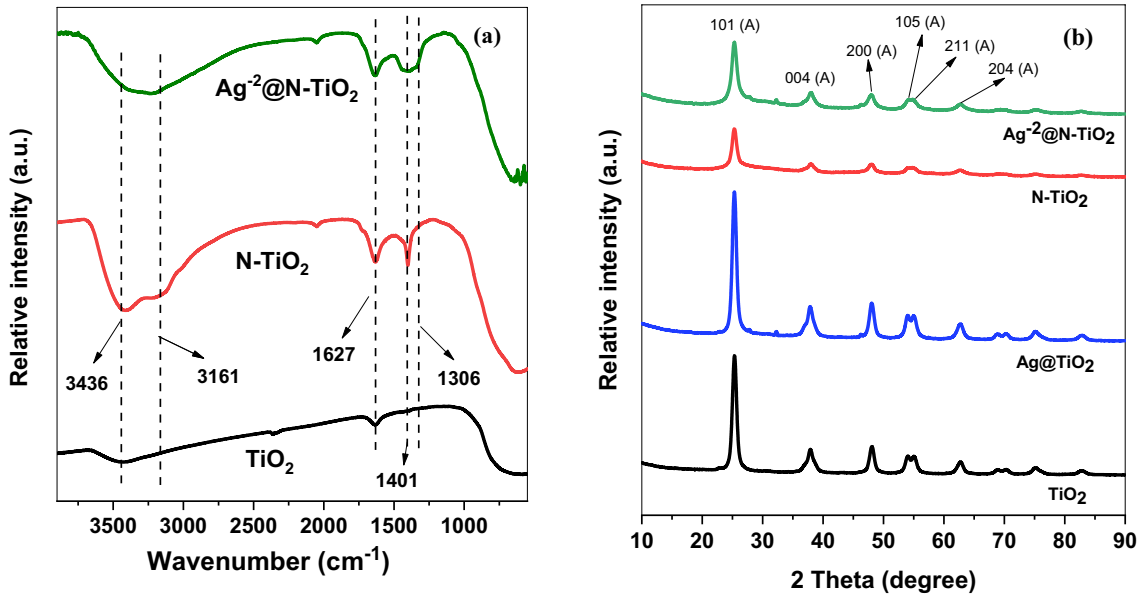

Fig. 1 **a** FTIR spectra and **b** XRD patterns of the prepared samples

addition, another characteristic peak is found at 3161 cm^{-1} and 3436 cm^{-1}, which correspond to the N-H stretching. Therefore, it implies that the N dopant was successfully incorporated into the TiO_2 lattice (Li et al. 2010; Sanchez-Martinez et al. 2018). Furthermore, the characteristic peak of Ag can be seen around 1306 cm^{-1} for Ag@N-TiO_2 samples. This peak indicates the interaction between Ag and TiO_2 which does not appear in the TiO_2 and N-TiO_2 (Sarteep et al. 2016).

Figure 1b shows the structural characteristics of the synthesized samples. It can be seen that bare TiO_2 consisted of an anatase crystalline phase. The diffraction peaks located at 2θ of 25.4°, 37.8°, 48.0°, 54.1°, 55.0°, and 62.7° corresponded to the (101), (004), (200), (105), (211), and (204) crystal faces of anatase TiO_2 (JCPDS, No.21-1272), respectively (Wang et al. 2017). No additional peaks were found at the crystal phase or structure of TiO_2 after modifications with N, Ag, and Ag@N/. It could be attributed to the fact that doping with N or/and Ag did not aggregate to form a new phase and did not alter the crystal structure of TiO_2 at low concentrations of dopants (< 10 wt%) (Chen et al. 2017; Abbad et al. 2020).

The average crystallite size was calculated from the diffraction pattern by using Scherrer's equation. The considered peaks for this calculation are at 2θ of 25, 37, and 48°, as shown in Table 1. The results show that the average crystallite size slightly decreased when it doped with N or/and Ag which is in agreement with the previous results (Pino-Sandoval et al. 2020; Abbad et al. 2020).

The optical properties of the synthesized samples were measured using a UV–Vis diffuse reflectance spectrophotometer as shown in Fig. 2. It can be seen that the absorption edge of TiO_2 moved to the visible region (redshift) after doping with N or/and Ag elements. The N dopant could produce a new energy level above the valence band of the TiO_2 and narrow the bandgap energy (Khan et al. 2014; Lei et al. 2015). In addition, the Ag modification also could change the energy level and increase the visible light absorption via the surface plasmon resonance effect (Chen et al. 2017). Yang et al. reported the fabrication of rice-like Ag@N-TiO_2 via hydrothermal and photoreduction methods. The optical properties also showed a redshift absorption of the N-TiO_2 and Ag@N-TiO_2 samples (Yang et al. 2016).

Table 1 Average crystallite size of the prepared samples

Catalysts	Peak position (2θ)	Crystallite size (nm)	Average crystallite size (nm)
TiO_2	25.319	11	14.17
	37.87	15.5	
	48.00	16	
N-TiO_2	25.311	11.6	11.73
	37.843	13.5	
	48.082	10.1	
Ag^{-2}@TiO_2	25.417	11.6	11.73
	37.799	13.5	
	48.012	10.1	
Ag^{-2}@N-TiO_2	25.305	11.6	11.73
	38.035	13.5	
	48.131	10.1	

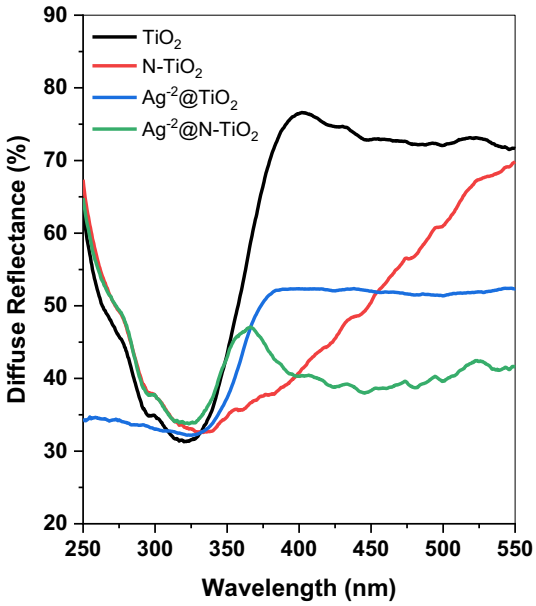

Fig. 2 Diffuse reflectance spectra of the prepared samples

Figure 3 shows the FE-SEM images of prepared samples. $Ag^{-2}@TiO_2$ and $Ag^{-2}@N\text{-}TiO_2$ nanocomposites were spherical in shape with a slight agglomeration (Fig. 3a and d). The particle size distribution was then calculated from FE-SEM images by using ImageJ software. The result shows that the particle sizes of $Ag^{-2}@TiO_2$ and $Ag^{-2}@N\text{-}TiO_2$ samples were around 160–300 nm but dominantly at 220–240 nm as shown in Fig. 4. Sun and co-workers also modified the TiO_2 with N and Ag nanoparticles via in situ calcination. Spherical nanoparticles were obtained using the synthesis method with a particle size of $Ag@N\text{-}TiO_2$ was about 63.5 nm (Sun et al. 2016).

Furthermore, small size and aggregated Ag nanoparticles were observed in both $Ag^{-2}@TiO_2$ (Fig. 3b, c) and $Ag^{-2}@N\text{-}TiO_2$ (Fig. 3e, f) nanocomposites. The dominant sizes of Ag nanoparticles were about 70–90 nm and 40–70 nm for $Ag^{-2}@TiO_2$ and $Ag^{-2}@N\text{-}TiO_2$, respectively (Fig. 5a, b). The present study possessed a larger Ag size distribution compared to the previously reported article (Sun et al. 2016). It implies that during the photochemical process by UV light irradiation, the high reduction potential of Ag^+ (0.799 V) accepted the photogenerated electron from CB of TiO_2 or $N\text{-}TiO_2$ and produced Ag^0 nanoparticles (Bhardwaj et al. 2019).

The EDX analysis was examined to investigate the elemental composition of the samples as shown in Figs. 6 and 7. Figures 6a–d and 7a–d show that Ti, O, and Ag elements were well distributed in all samples of $Ag^{-2}@TiO_2$ and $Ag^{-2}@N\text{-}TiO_2$ nanocomposites. However, some Ag nanoparticles were aggregated in some areas which are indicated by a thicker blue color of Ag element. Compared to $Ag^{-2}@TiO_2$ (Fig. 6d), more Ag aggregations were found in the $Ag^{-2}@N\text{-}TiO_2$ sample (Fig. 7d). This phenomenon might be due to the long irradiation time of the photochemical reaction which continuously produces Ag^0 nanoparticles and then agglomeration (Bhardwaj et al. 2019). Furthermore, the Ag element also had been detected in the EDX spectra at around 3 keV for $Ag^{-2}@TiO_2$ and $Ag^{-2}@N\text{-}TiO_2$ samples (Figs. 6e and 7e). It implies that Ag was successfully incorporated into TiO_2. However, the atomic percentage of Ag in the $Ag^{-2}@TiO_2$ sample was higher compared to that of $Ag^{-2}@N\text{-}TiO_2$ with values of 7.7% and 1.3%, respectively.

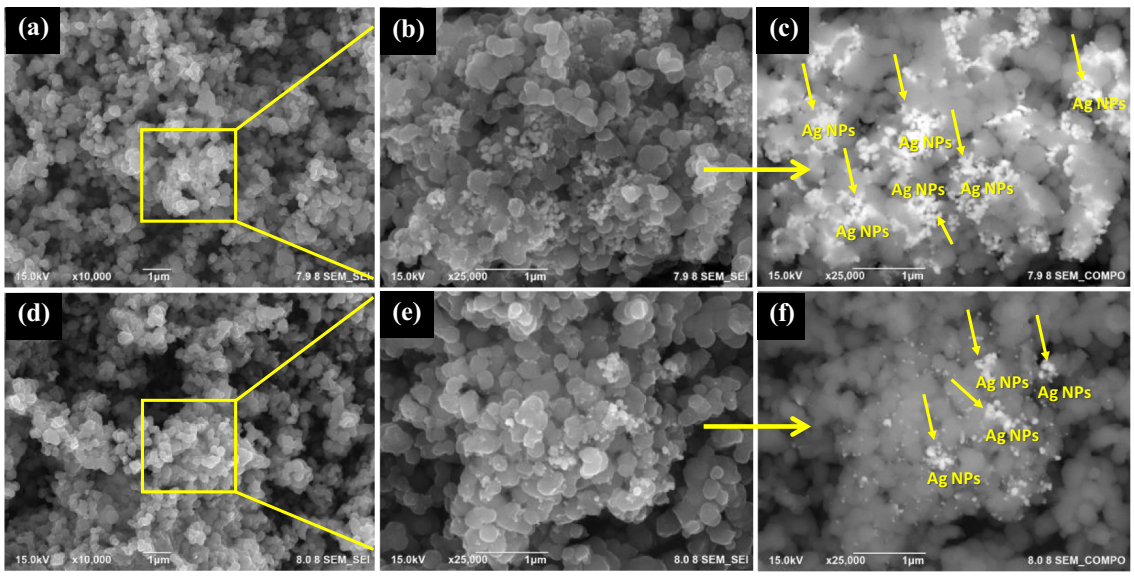

Fig. 3 FE-SEM images of **a–c** $Ag^{-2}@TiO_2$ and **d–f** $Ag^{-2}@N\text{-}TiO_2$ nanocomposites

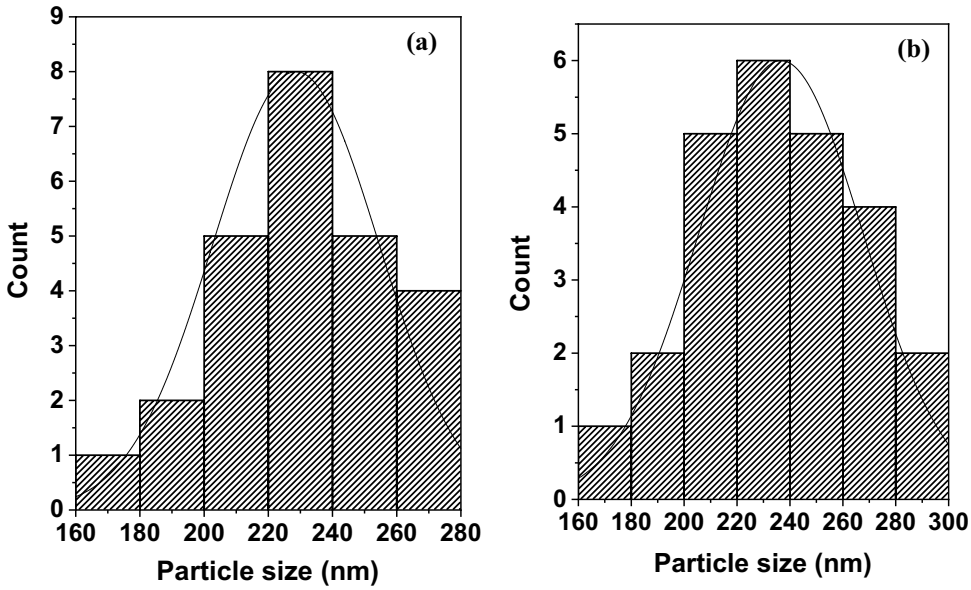

Fig. 4 Particle size distribution of **a** $Ag^{-2}@TiO_2$ and **b** $Ag^{-2}@N\text{-}TiO_2$ nanocomposites

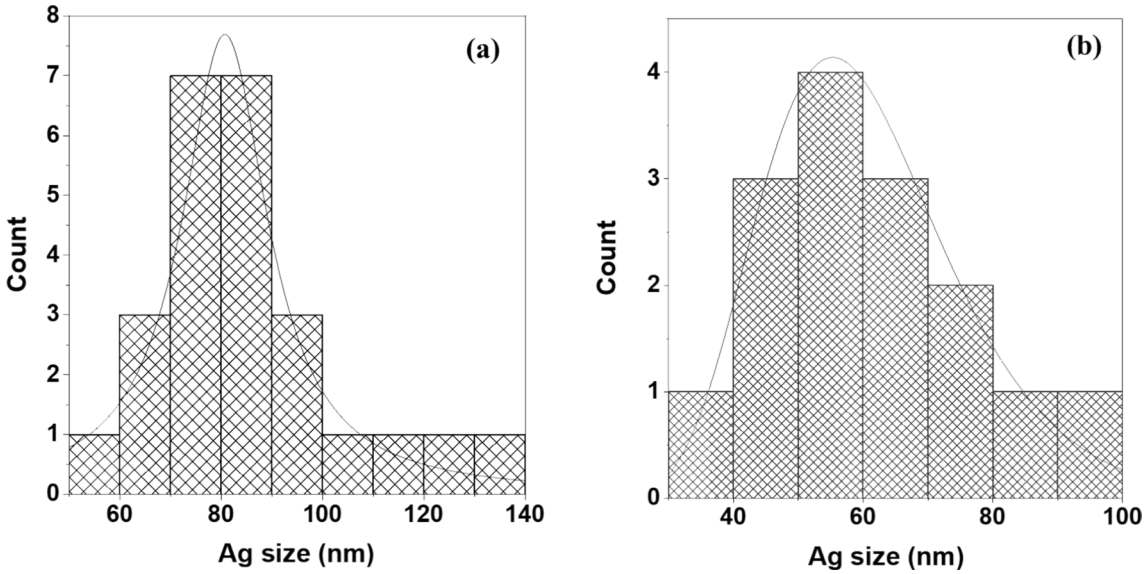

Fig. 5 Average Ag size attached onto the surface of **a** TiO_2 and **b** $N\text{-}TiO_2$ composites

In addition, the N content in the $Ag^{-2}@N\text{-}TiO_2$ sample could not be detected by EDX analysis. It might be due to the sensitivity limit of the EDX device and a very small amount of N atoms infiltrating the crystal structure of TiO_2 (Chen et al. 2017).

Bacterial identification and susceptibility assays of MDR *K. pneumoniae*

Bacterial samples were inoculated on MacConkey agar plates and appear some mucoid pink-colored colonies after 24 h at 37 °C incubation. Microscopic observation through Gram staining procedure successfully identified a rod-shape magenta red-colored gram-negative bacteria (Fig. 8). The result of the biochemical identification test using Microbact® GNB 12A completed evidence that the bacterial sample was identified as *Klebsiella pneumoniae* (Table 2).

Antibiotic susceptibility test

Susceptibility of *K. pneumoniae* against several antibiotics was performed by a disc diffusion method on a Mueller–Hinton (MH) agar medium (Matuschek et al. 2014). Five different types of antibiotics: amoxicillin/

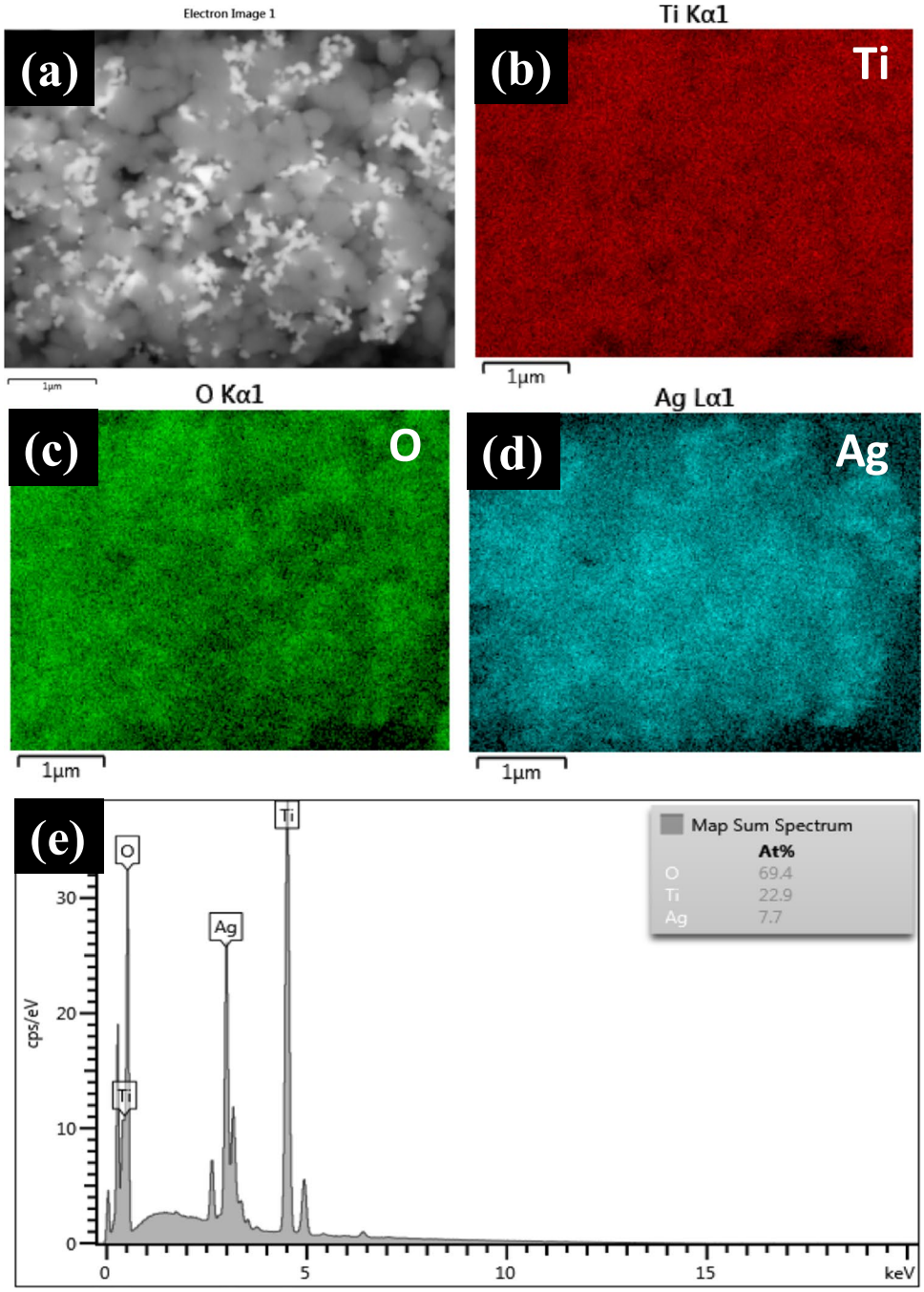

Fig. 6 **a**–**d** EDX elemental mapping and **e** EDX spectra Ag^{-2}@TiO_2 nanocomposite

AML (25 µg), cefixime/CFM (10 µg), cefotaxime/CTX (30 µg), cefuroxime/CXM (30 µg), and ceftriaxone/CXO (30 µg) were selected. Antibiotic selections, dosage, and methods were adopted as mentioned in EUCAST clinical breakpoint table for antimicrobial susceptibility testing (EUCAST 2022). According to the EUCAST table of clinical breakpoint v.13.1, bacterial samples were resistant to all selected antibiotics (Fig. 9), thus can be categorized as multidrug-resistant (MDR) strains (Khasanah et al. 2020; EUCAST 2022).

Antimicrobial activity of Ag@TiO_2 and Ag@N-TiO_2 nanocomposites against MDR *K. pneumoniae*

The antimicrobial assay was conducted using the Kirby-Bauer disc diffusion method against MDR *K. pneumoniae*. Inhibition zone (mm) by Ag@TiO_2 and Ag@N-TiO_2 nanocomposites with various Ag concentrations is shown in Table 3 and Fig. 10.

Figure 10 shows the photograph of the inhibition zone produced by various concentrations of Ag@TiO_2 and

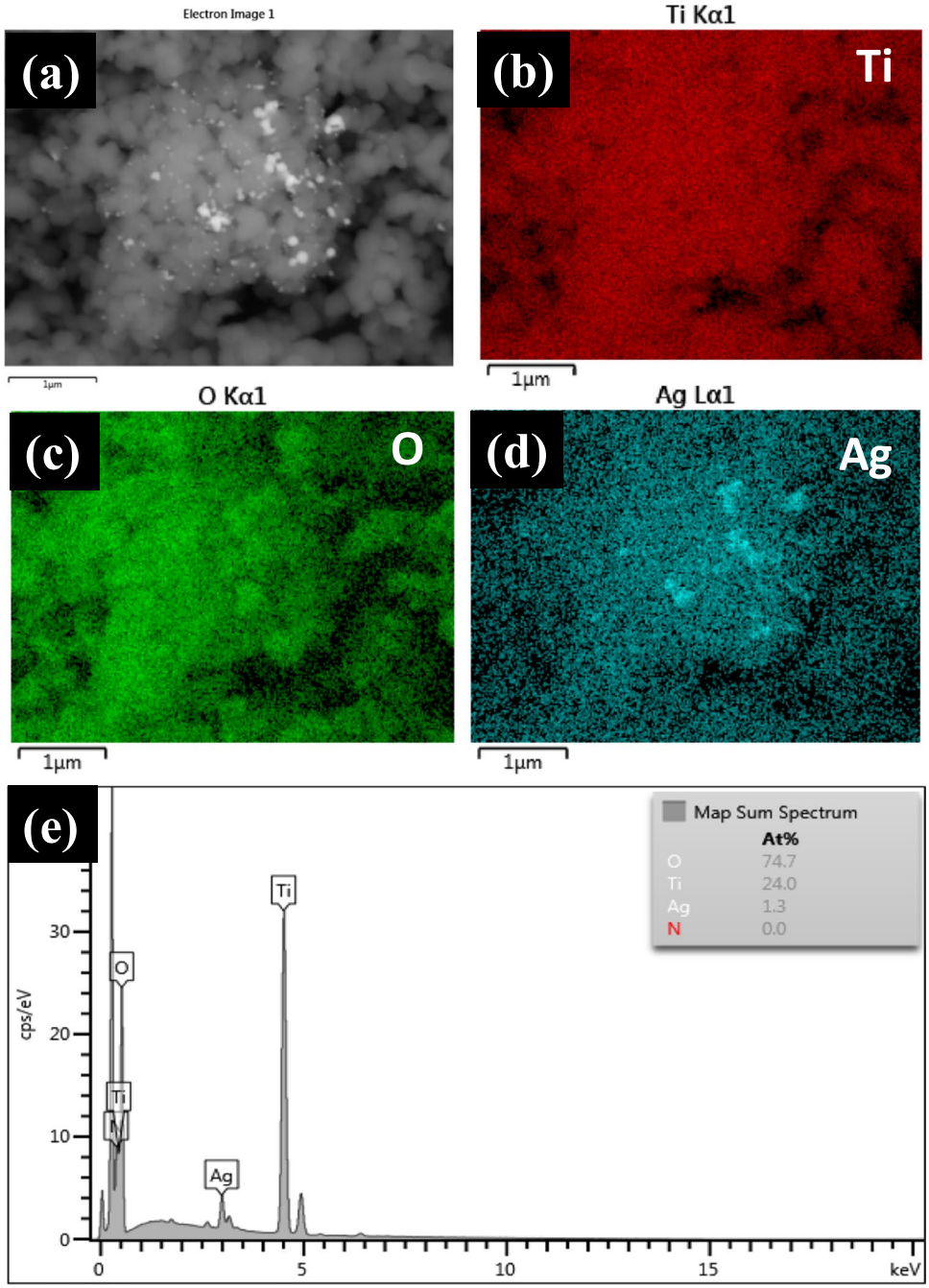

Fig. 7 **a**–**d** EDX elemental mapping and **e** EDX spectra Ag^{-2}@N-TiO_2 nanocomposite

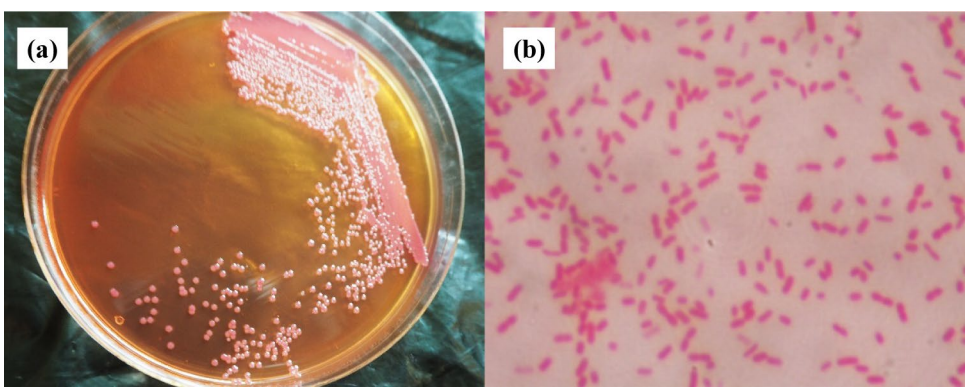

Fig. 8 **a** Colony and **b** cell morphology of *Klebsiella pneumoniae* after Gram staining

Table 2 Biochemical identification of *K. pneumoniae* isolated sample using Microbact® GNB 12A after 24 h incubation

S. No.	Biochemical reaction	Results
1	Lysine decarboxylase	Positive
2	Ornithine decarboxylase	Negative
3	H_2S production	Negative
4	Glucose fermentation	Positive
5	Mannitol fermentation	Positive
6	Xylose fermentation	Positive
7	Hydrolysis of o-nitrophenyl-ß-d-galactopyranoside (ONPG) by ß-galactosidase	Positive
8	Production of indole from tryptophan	Negative
9	Hydrolysis of urea	Positive
10	Production of acetoin from Voges–Proskaüer reaction	Positive
11	Citrate metabolism	Positive
12	Production of indole-pyruvate from tryptophan deamination	Negative

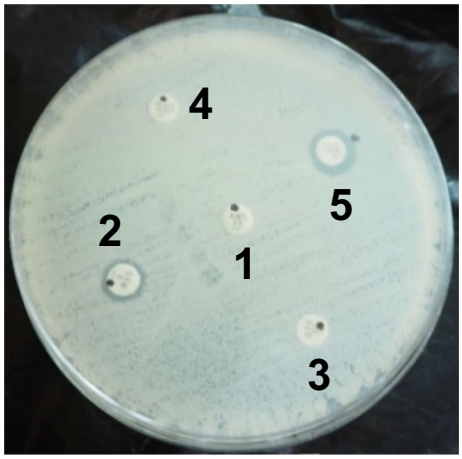

Fig. 9 Susceptibility test result of several antibiotics: (1) AML, (2) CFM, (3) CTX, (4) CXM, and (5) CXO against *K. pneumoniae*

Table 3 Inhibition zone of Ag@TiO_2 and Ag@N-TiO_2 nanocomposites

Samples	Inhibition zone (mm)			Mean ± SD	Inhibition zone (%)
	I	II	III		
(+) control	3.62	3.45	3.77	3.61 ± 0.16	100
Ag^{-3}@TiO_2	2.72	2.85	2.80	2.79 ± 0.06	77.29
Ag^{-2}@TiO_2	2.68	2.80	2.69	2.72 ± 0.07	75.35
Ag^{-1}@TiO_2	2.71	2.65	2.68	2.68 ± 0.03	74.24
Ag^{-3}@N-TiO_2	2.50	2.55	2.35	2.47 ± 0.10	68.42
Ag^{-2}@N-TiO_2	1.80	1.84	1.87	1.84 ± 0.03	50.97
Ag^{-1}@N-TiO_2	1.35	1.28	1.34	1.32 ± 0.04	36.57
(−) control	0.11	0.12	0.10	0.11 ± 0.01	3.05

Ag@N-TiO_2 nanocomposites against MDR *K. pneumoniae*. All experimental groups were significantly different against negative control with the value of $P \leq 0{,}05$ according to the one-way ANOVA significance test. It means that all nanocomposites actively inhibited the growth of MDR *K. pneumoniae*. Moreover, post hoc (Tukey) test revealed that the increasing of Ag concentration on Ag@TiO_2 nanocomposites exhibited no impact on the antimicrobial activity. On the other hand, a significant decline was recorded for Ag@N-TiO_2 samples at higher Ag concentration ($P \leq 0{,}05$). The details of statistical analysis are shown in Tables S1, S2 in the Supplementary Information. From the result, Ag@TiO_2 exhibited more antimicrobial activity compared to Ag@N-TiO_2. Conversely, an elevation in the concentration of silver (Ag) resulted in a decrease in the antimicrobial activity of nanoparticles against MDR *K. pneumoniae*. Ag^{-3}@TiO_2 nanocomposite exhibited maximum zone inhibition (2.79 ± 0.06 mm or 77.29%), while Ag^{-1}@N-TiO_2 nanocomposite showed minimum zone of inhibition (1.32 ± 0.04 mm or 36.57%) as shown in Table 3 and Fig. 11.

Previous antimicrobial studies have been made for Ag@TiO_2 and Ag@N-TiO_2 nanocomposites against *Escherichia coli, Streptococcus pyogenes, Staphylococcus aureus,* and *Acinetobacter baumannii* (Wong et al. 2015). However, the antimicrobial properties of Ag nanoparticles along with TiO_2 are reported to be more effective in the presence of visible light (Khan et al. 2019). TiO_2 exhibited a photocatalytic activity with Ag to produce *reactive oxygen species* (ROS) ($O_2^{\cdot-}$ and $^{\cdot}OH$). The addition of a nitrogen (N) atom could enhance the reaction by reducing its activation energy (Schneider et al. 2014; Ansari et al. 2016; Yang et al. 2018).

Anti-biofilm activity

The ability of Ag@TiO_2 and Ag@N-TiO_2 nanocomposites to tackle the biofilm formation of MDR *K. pneumoniae* was evaluated with the tissue culture plate method using crystal violet staining (Roy et al. 2018). A bacterial culture

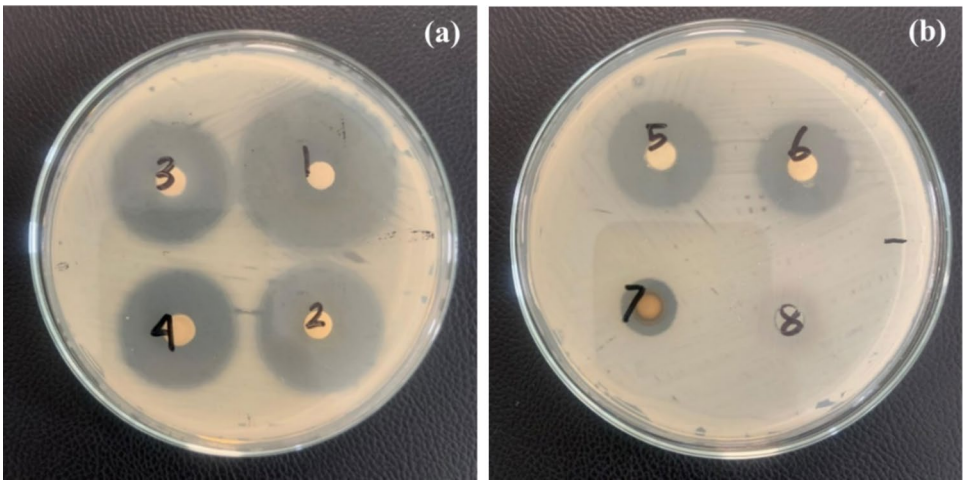

Fig. 10 The photograph of inhibition zone produced by Ag@TiO_2 and Ag@N-TiO_2 samples: (1) (+) control; (2) Ag^{-3}@TiO_2; (3) Ag^{-2}@TiO_2; (4) Ag^{-1}@TiO_2; (5) Ag^{-3}@N-TiO_2; (6) Ag^{-2}@N-TiO_2; (7) Ag^{-1}@N-TiO_2; and (8) (−) control

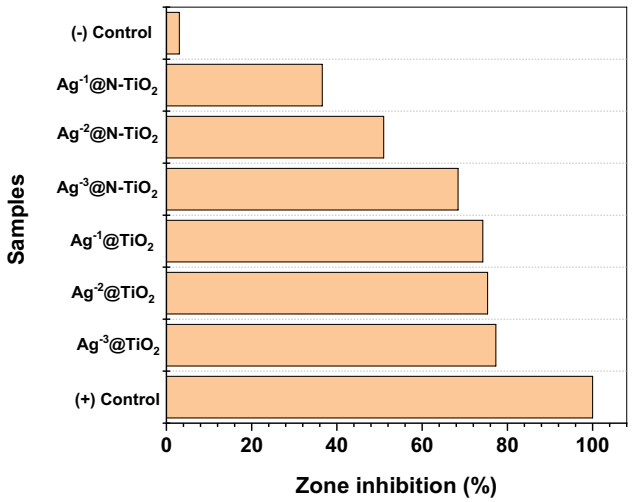

Fig. 11 Inhibition zone (%) of MDR *K. pneumoniae* introduced by various silver concentrations of Ag@TiO_2 and Ag@N-TiO_2 nanocomposites

was inoculated on the surface of silicone material to mimic the biofilm formation on a silicone catheter. Anti-biofilm test results revealed that both Ag@TiO_2 and Ag@N-TiO_2 nanoparticles acted as good anti-biofilm agents against MDR *K. pneumoniae*. Table 4 and Fig. 12 show the percentage of anti-biofilm inhibition of Ag@TiO_2 and Ag@N-TiO_2 nanocomposites in various concentrations.

Anti-biofilm activity of Ag@TiO_2 and Ag@N-TiO_2 nanocomposites was decreased in the addition of Ag. Ag^{-1}@TiO_2 nanocomposite exhibited optimum anti-biofilm effect with 54.206% of inhibition after the positive control (meropenem 10 µg; 61.682%). Our finding revealed that both Ag@TiO_2 and Ag@N-TiO_2 nanocomposites were good anti-biofilm agents. The statistical analysis of the one-way ANOVA and post hoc (Tukey)

Table 4 Biofilm inhibition of Ag@TiO_2 and Ag@N-TiO_2 nanocomposites against MDR *K. pneumoniae* on silicone material

Samples	Optical density at 595 nm wavelength (OD_{595})			Mean ± SD	Biofilm inhibition (%)
	I	II	III		
(−) control	0.466	0.456	0.362	0.428 ± 0.574	0.000
Ag^{-1}@N-TiO_2	0.375	0.249	0.341	0.322 ± 0.065	24.844
Ag^{-2}@N-TiO_2	0.328	0.267	0.261	0.285 ± 0.037	33.333
Ag^{-3}@N-TiO_2	0.288	0.227	0.226	0.247 ± 0.035	42.290
Ag^{-1}@TiO_2	0.225	0.175	0.187	0.196 ± 0.026	54.283
Ag^{-2}@TiO_2	0.307	0.295	0.285	0.296 ± 0.011	30.919
Ag^{-3}@TiO_2	0.320	0.232	0.265	0.272 ± 0.044	36.371
(+) control	0.162	0.190	0.140	0.164 ± 0.025	61.682

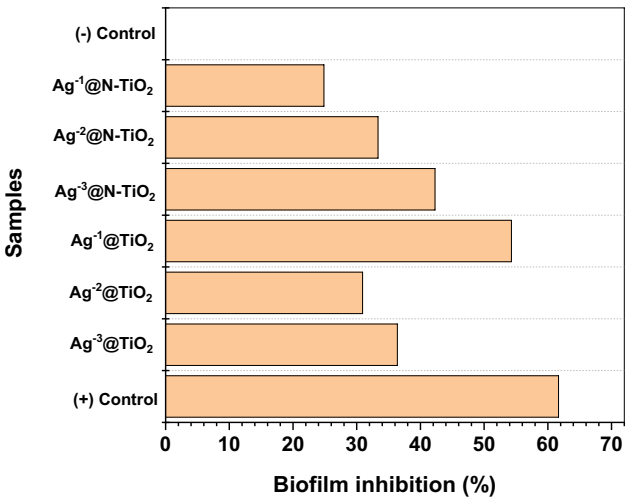

Fig. 12 Biofilm inhibition (%) of Ag@TiO_2 and Ag@N-TiO_2 nanocomposites against MDR *K. pneumoniae* on the silicone material

tests also showed a significantly different against negative control with the value of $P \leq 0{,}05$ (see Tables S3, S4).

Interestingly, Swidan and his co-workers reported that Ag nanoparticles inhibited biofilm formation by disrupting the intermolecular forces between bacterial cells with some abiotic surfaces. Ag nanoparticles exhibited anti-quorum sensing activities against the biofilm formation of pathogens (Santhosh and Natarajan 2015; Swidan et al. 2022). Another experiment also reported the anti-biofilm and antimicrobial activities of Ag@TiO_2 and Ag@N-TiO_2 nanocomposites were affected by some factors, i.e., particle size and distribution, degree of agglomeration, the concentration of Ag, and interaction with target molecules (Jalali et al. 2016).

Additionally, our results also revealed that an excessive $AgNO_3$ concentration could increase the aggregation and agglomeration of the produced Ag nanoparticles which then reduce its surface area (Chakhtouna et al. 2021). This phenomenon could affect to the interaction between active materials with target bacteria and decreased the antimicrobial and anti-biofilm activities (Murugadoss et al. 2020). On the other hand, the presence of nitrogen doping on Ag@N-TiO_2 resulted a lower percentage of Ag nanoparticle as an active microbial agent (1.3%) compared to Ag@TiO_2 (7.7%) as shown in the EDX result in Figs. 6 and 7. As a result, the presence of nitrogen doping could not significantly affect to enhance the antimicrobial activity (Lan et al. 2013). Overall, the prepared nanocomposites still showed a great promise as antimicrobial and anti-biofilm agents against MDR *K. pneumoniae* but require more scientific evidence on the study of in vivo.

Conclusion

Herein, we report the successful synthesis of spherical TiO_2, N-TiO_2, Ag@TiO_2, and Ag@N-TiO_2 nanocomposites via the sol–gel and photochemical reduction methods. XRD patterns showed that all samples were in the anatase phase. FE-SEM and EDX results showed that Ag nanoparticles have been successfully decorated on the surface of TiO_2 and N-TiO_2. Furthermore, both Ag@TiO_2 and Ag@N-TiO_2 nanocomposites showed antimicrobial and anti-biofilm effects against multidrug resistance *K. pneumoniae* which was clinically isolated from a sputum specimen of pneumoniae-active patient. Our result suggests that silver concentration significantly affected the antimicrobial and anti-biofilm activities of Ag@TiO_2 and Ag@N-TiO_2 nanocomposites. Furthermore, Ag@TiO_2 and Ag@N-TiO_2 nanocomposites potentially offer a promising inert antimicrobial and anti-biofilm coating agent for medical devices to control the spreading of biofilm associated with the MDR *K. pneumoniae*.

Supplementary Information The online version contains supplementary material available at https://doi.org/10.1007/s11696-024-03737-3.

Acknowledgements Authors would like to acknowledge to "Laboratorium Imaging Fisika Maju" at the National Research and Innovation Agency (BRIN) for instrumental measurements of XRD, FTIR, FE-SEM, and EDX.

Author contributions AFF contributed to conceptualization, data curation, formal analysis, methodology, investigation, visualization, writing—original draft, and resource. LR contributed to investigation, data curation, and visualization. MMK contributed to formal analysis, validation, and writing—review & editing. AW contributed to conceptualization, data curation, formal analysis, methodology, investigation, visualization, writing—original draft, validation, writing—review & editing, and resource.

Funding This work was funded by LPPM Universitas Islam Negeri Maulana Malik Ibrahim Malang, Indonesia, through Bantuan Operasional Perguruan Tinggi Negeri (BOPTN) Litapdimas with contract number of 1081A/LP2M/PPK/TL.00/03/2023. Additionally, this work was partly supported by the Research Organization for Nanotechnology and Materials – National Research and Innovation Agency (BRIN) .

Data availability No datasets were generated during the current study.

Declarations

Conflict of interest The authors have no competing interests to declare that are relevant to the content of this article.

Ethical approval Not applicable.

Research involving humans and animals statement None.

References

Abbad S, Guergouri K, Gazaout S et al (2020) Effect of silver doping on the photocatalytic activity of TiO_2 nanopowders synthesized by the sol-gel route. J Environ Chem Eng 8:103718. https://doi.org/10.1016/j.jece.2020.103718

Adeosun IJ, Baloyi IT, Cosa S (2022) Anti-biofilm and associated anti-virulence activities of selected phytochemical compounds against *Klebsiella pneumoniae*. Plants (Basel) 11:1429. https://doi.org/10.3390/plants11111429

Alotaibi AM, Alsaleh NB, Aljasham AT et al (2022) Silver nanoparticle-based combinations with antimicrobial agents against antimicrobial-resistant clinical isolates. Antibiotics (Basel) 11:1219. https://doi.org/10.3390/antibiotics11091219

Ansari SA, Khan MM, Ansari MO, Cho MH (2016) Nitrogen-doped titanium dioxide (N-doped TiO_2) for visible light photocatalysis. New J Chem 40:3000–3009. https://doi.org/10.1039/C5NJ03478G

Bhardwaj S, Dogra D, Pal B, Singh S (2019) Photodeposition time dependant growth, size and photoactivity of Ag and Cu deposited TiO_2 nanocatalyst under solar irradiation. Sol Energy 194:618–627. https://doi.org/10.1016/j.solener.2019.10.055

Calisir MD, Gungor M, Demir A et al (2020) Nitrogen-doped TiO_2 fibers for visible-light-induced photocatalytic activities. Ceram Int 46:16743–16753. https://doi.org/10.1016/j.ceramint.2020.03.250

CDC (2024) Urinary tract infection (Catheter-associated urinary tract infection [CAUTI] and non-catheter-associated urinary tract infection [UTI]) Events, https://www.cdc.gov/nhsn/pdfs/pscmanual/7psccauticurrent.pdf, accessed on 4th September 2024

Centeleghe I, Norville P, Hughes L, Maillard J-Y (2023) *Klebsiella pneumoniae* survives on surfaces as a dry biofilm. Am J Infect Control 51:1157–1162. https://doi.org/10.1016/j.ajic.2023.02.009

Chakhtouna H, Benzeid H, Zari N et al (2021) Recent progress on Ag/TiO_2 photocatalysts: photocatalytic and bactericidal behaviors. Environ Sci Pollut Res 28:44638–44666. https://doi.org/10.1007/s11356-021-14996-y

Chang D, Sharma L, Dela Cruz CS, Zhang D (2021) Clinical epidemiology, risk factors, and control strategies of *Klebsiella pneumoniae* infection. Front Microbiol 12:750662. https://doi.org/10.3389/fmicb.2021.750662

Chen Q, Zhang Y, Zhang D, Yang Y (2017) Ag and N co-doped TiO_2 nanostructured photocatalyst for printing and dyeing wastewater. J Water Process Eng 16:14–20. https://doi.org/10.1016/j.jwpe.2016.11.007

Cheng X, Yu X, Xing Z, Yang L (2016) Synthesis and characterization of N-doped TiO_2 and its enhanced visible-light photocatalytic activity. Arab J Chem 9:S1706–S1711. https://doi.org/10.1016/j.arabjc.2012.04.052

Donlan RM (2002) Biofilms: microbial life on surfaces. Emerg Infect Dis 8:881–890. https://doi.org/10.3201/eid0809.020063

EUCAST (2022) Clinical breakpoints–breakpoints and guidance. 15, https://www.eucast.org/clinical_breakpoints, Accessed on 4th September 2024.

Jalali SAH, Allafchian AR, Banifatemi SS, Ashrafi Tamai I (2016) The antibacterial properties of Ag/TiO_2 nanoparticles embedded in silane sol–gel matrix. J Taiwan Inst Chem Eng 66:357–362. https://doi.org/10.1016/j.jtice.2016.06.011

Khan MM, Kalathil S, Lee J-T, Cho M-H (2012) Synthesis of cysteine capped silver nanoparticles by electrochemically active biofilm and their antibacterial activities. Bull Korean Chem Soc 33:2592–2596. https://doi.org/10.5012/bkcs.2012.33.8.2592

Khan MM, Ansari SA, Pradhan D et al (2014) Band gap engineered TiO_2 nanoparticles for visible light induced photoelectrochemical and photocatalytic studies. J Mater Chem A 2:637–644. https://doi.org/10.1039/C3TA14052K

Khan AU, Khan M, Khan MM (2019) Antifungal and antibacterial assay by silver nanoparticles synthesized from aqueous leaf extract of *Trigonella foenum-graecum*. Bionanoscience 9:597–602. https://doi.org/10.1007/s12668-019-00643-x

Khasanah RN, Puspitasari I, Nuryastuti T, Yuniarti N (2020) Prevalensi Multidrug-Resistant Klebsiella pneumonia dan Evaluasi Kesesuaian Antibiotik Empiris Berdasarkan Nilai Prediksi Farmakokinetik Terhadap Outcome Klinis di RSUP Dr. Soeradji Tirtonegoro Klaten. Majalah Farmaseutik 16:27–33. https://doi.org/10.22146/farmaseutik.v16i1.47914

Lan M-Y, Liu C-P, Huang H-H, Lee S-W (2013) Both enhanced biocompatibility and antibacterial activity in Ag-decorated TiO_2 nanotubes. PLoS ONE 8:e75364. https://doi.org/10.1371/journal.pone.0075364

Lei XF, Xue XX, Yang H et al (2015) Effect of calcination temperature on the structure and visible-light photocatalytic activities of (N, S and C) co-doped TiO_2 nano-materials. Appl Surf Sci 332:172–180. https://doi.org/10.1016/j.apsusc.2015.01.110

Li Y, Jiang Y, Peng S, Jiang F (2010) Nitrogen-doped TiO_2 modified with NH_4F for efficient photocatalytic degradation of formaldehyde under blue light-emitting diodes. J Hazard Mater 182:90–96. https://doi.org/10.1016/J.JHAZMAT.2010.06.002

Li Y, Kumar S, Zhang L, Wu H (2022) *Klebsiella pneumonia* and its antibiotic resistance: a bibliometric analysis. Biomed Res Int 2022:1668789. https://doi.org/10.1155/2022/1668789

Matuschek E, Brown DFJ, Kahlmeter G (2014) Development of the EUCAST disk diffusion antimicrobial susceptibility testing method and its implementation in routine microbiology laboratories. Clin Microbiol Infect 20:O255–O266. https://doi.org/10.1111/1469-0691.12373

Murugadoss S, Brassinne F, Sebaihi N et al (2020) Agglomeration of titanium dioxide nanoparticles increases toxicological responses in vitro and in vivo. Part Fibre Toxicol 17:10. https://doi.org/10.1186/s12989-020-00341-7

Naik K, Kowshik M (2014) Anti-quorum sensing activity of AgCl-TiO_2 nanoparticles with potential use as active food packaging material. J Appl Microbiol 117:972–983. https://doi.org/10.1111/jam.12589

Ocwelwang AR, Tichagwa L (2014) Synthesis and characterisation of Ag and nitrogen doped TiO_2 nanoparticles supported on a Chitosan-Pvae nanofibre support. Int J Adv Res Chem Sci 1:28–37

Osman EA, El-Amin N, Adrees EAE et al (2020) Comparing conventional, biochemical and genotypic methods for accurate identification of *Klebsiella pneumoniae* in Sudan. Access Microbiol 2:acmi000096. https://doi.org/10.1099/acmi.0.000096

Pino-Sandoval D, Villanueva-Rodríguez M, Cantú-Cárdenas ME, Hernández-Ramírez A (2020) Performance of Ag-Cu/TiO_2 photocatalyst prepared by sol-gel method on the inactivation of *Escherichia coli* and *Salmonella typhimurium*. J Environ Chem Eng 8:104539. https://doi.org/10.1016/j.jece.2020.104539

Roy R, Tiwari M, Donelli G, Tiwari V (2018) Strategies for combating bacterial biofilms: a focus on anti-biofilm agents and their mechanisms of action. Virulence 9:522–554. https://doi.org/10.1080/21505594.2017.1313372

Sanchez-Martinez A, Ceballos-Sanchez O, Koop-Santa C et al (2018) N-doped TiO_2 nanoparticles obtained by a facile coprecipitation method at low temperature. Ceram Int 44:5273–5283. https://doi.org/10.1016/j.ceramint.2017.12.140

Santhosh S, Natarajan K (2015) Antibiofilm activity of Epoxy/Ag-TiO_2 polymer nanocomposite coatings against *Staphylococcus aureus* and *Escherichia coli*. Coatings 5:95–114. https://doi.org/10.3390/coatings5020095

Sarteep Z, Pirbazari AE, Aroon MA (2016) Silver doped TiO_2 nanoparticles: preparation, characterization and efficient degradation of 2,4-dichlorophenol under visible light. Nanotechnol J Water Environ Nanotechnol 1:135–144. https://doi.org/10.7508/jwent.2016.02.007

Schneider J, Matsuoka M, Takeuchi M et al (2014) Understanding TiO_2 photocatalysis: mechanisms and materials. Chem Rev 114:9919–9986. https://doi.org/10.1021/cr5001892

Sun M, Fang Y, Sun S, Wang Y (2016) Surface co-modification of TiO_2 with N doping and Ag loading for enhanced visible-light photoactivity. RSC Adv 6:12272–12279. https://doi.org/10.1039/c5ra23593f

Swidan NS, Hashem YA, Elkhatib WF, Yassien MA (2022) Antibiofilm activity of green synthesized silver nanoparticles against biofilm associated enterococcal urinary pathogens. Sci Rep 12:3869. https://doi.org/10.1038/s41598-022-07831-y

Tacconelli E, Carrara E, Savoldi A et al (2018) Discovery, research, and development of new antibiotics: the WHO priority list of antibiotic-resistant bacteria and tuberculosis. Lancet Infect Dis 18:318–327. https://doi.org/10.1016/S1473-3099(17)30753-3

Wafi A, Szabó-Bárdos E, Horváth O et al (2020) The photocatalytic and antibacterial performance of nitrogen-doped TiO_2: surface-structure dependence and silver-deposition effect. Nanomaterials 10:1–19. https://doi.org/10.3390/nano10112261

Wang T, Wei J, Shi H et al (2017) Preparation of electrospun Ag/TiO_2 nanotubes with enhanced photocatalytic activity based on water/oil phase separation. Physica E Low Dimens Syst Nanostruct 86:103–110. https://doi.org/10.1016/j.physe.2016.10.016

Wong M-S, Chen C-W, Hsieh C-C et al (2015) Antibacterial property of Ag nanoparticle-impregnated N-doped titania films under visible light. Sci Rep 5:11978. https://doi.org/10.1038/srep11978

Yang S, Wang H, Yu H et al (2016) A facile fabrication of hierarchical Ag nanoparticles-decorated N-TiO_2 with enhanced photocatalytic hydrogen production under solar light. Int J Hydrogen Energy 41:3446–3455. https://doi.org/10.1016/j.ijhydene.2015.12.190

Yang G, Yin H, Liu W et al (2018) Synergistic Ag/TiO_2-N photocatalytic system and its enhanced antibacterial activity towards *Acinetobacter baumannii*. Appl Catal B 224:175–182. https://doi.org/10.1016/j.apcatb.2017.10.052